

Electrohydrodynamic Jet Printing of 1D Photonic Crystals: Part II—Optical Design and Reflectance Characteristics

Brian Iezzi, Zahra Afkhami, Shea Sanvordenker, David Hoelzle, Kira Barton, and Max Shtein*

Additive manufacturing systems that can arbitrarily deposit multiple materials into precise, 3D spaces spanning the micro- to nanoscale are enabling novel structures with useful thermal, electrical, and optical properties. In this companion paper set, electrohydrodynamic jet (e-jet) printing is investigated for its ability in depositing multimaterial, multilayer films with microscale spatial resolution and nanoscale thickness control, with a demonstration of this capability in creating 1D photonic crystals (1DPCs) with response near the visible regime. Transfer matrix simulations are used to evaluate different material classes for use in a printed 1DPC, and commercially available photopolymers with varying refractive indices ($n = 1.35$ to 1.70) are selected based on their relative high index contrast and fast curing times. E-jet printing is then used to experimentally demonstrate pixelated 1DPCs with individual layer thicknesses between 80 and 200 nm, square pixels smaller than $40\ \mu\text{m}$ across, with surface roughness less than 20 nm. The reflectance characteristics of the printed 1DPCs are measured using spatially selective microspectroscopy and correlated to the transfer matrix simulations. These results are an important step toward enabling cost-effective, custom-fabrication of advanced imaging devices or photonic crystal sensing platforms.

1. Introduction

Archetypal 1D photonic crystals (1DPCs) are comprised of alternating layers of high and low refractive index materials with an optical thickness on the order of the wavelength of

the incident light. As optical filters or mirrors, the transmittance or reflectance of light by these 1DPCs can be tuned by adjusting the sequence, thickness, and refractive index in the stack. 1DPCs have found wide ranging applications; from conventional lasers and optical filtering to novel mechanical and chemical sensing devices.^[1–5] 1DPCs have been fabricated by physical and chemical vapor deposition, solution processes such as spin- or dip-coating, and thermal drawing, among other methods.^[6–10] Polymeric 1DPCs in particular have attracted attention recently due to their potential for simplified processing, as well as freedom to design chemically and structurally derived capabilities for new sensory applications.^[11]

Creating arrays of 1DPC elements (pixel filters) typically requires many costly lithographic steps.^[12,13] For instance, arrays of 1DPCs for imaging applications with pixel sizes of $30\ \mu\text{m} \times 30\ \mu\text{m}$ were created with photolithographic masking processes, achieving a 2×2 array with each of the 4 pixels having a different optical response.^[14,15] Expanding to a larger multispectral or hyperspectral array with each element having a different response requires a corresponding increase in masking steps (i.e., 9 for a 3×3 array, 16 for a 4×4 , etc.). Since a different optical response also requires a different thickness for each layer within each pixel, the number of deposition steps scales at the same rate. It is therefore desirable to develop a mask-free, direct-deposition method that can achieve pixelated arrays of 1DPCs.^[16,17]


Emerging additive manufacturing (AM) processes have recently been applied to the creation of photonic crystals with single and multiple materials at various length scales. At the mesoscale, fused deposition printing and a photonic crystal block copolymer were combined to produce 3D objects with structural color.^[18] Several studies have also shown that multiple photopolymers could be used with digital light projection to create a single structure at the mesoscale.^[19,20] At smaller length scales of patterning, two-photon photopolymerization was used to realize air/polymer photonic crystals at the sub- μm length scale that achieved response in the visible regime after a postprint thermal shrinking procedure.^[21] While patterned arrays of photonic crystals have been demonstrated using inkjet printing, the need for solvent orthogonality and low viscosity inks have severely limited the structures obtained thus far.^[22]

B. Iezzi, Prof. M. Shtein
Department of Materials Science and Engineering
University of Michigan
Ann Arbor, MI 48109, USA
E-mail: mshtein@umich.edu

Z. Afkhami, Prof. K. Barton
Department of Mechanical Engineering
University of Michigan
Ann Arbor, MI 48109, USA

S. Sanvordenker
Department of Chemical Engineering
University of Michigan
Ann Arbor, MI 48109, USA

Prof. D. Hoelzle
Department of Mechanical and Aerospace Engineering
The Ohio State University
Columbus, OH 43210, USA

 The ORCID identification number(s) for the author(s) of this article can be found under <https://doi.org/10.1002/admt.202000431>.

DOI: 10.1002/admt.202000431

To enable the use of a range of photopolymerizable inks, which can have high viscosity (>500 cP), electrohydrodynamic jet (e-jet) printing is utilized. E-jet printing is a high-resolution AM technique that operates by applying an electric field between a conductive nozzle and a grounded substrate to generate extremely high shear forces on the fluid without additional wall friction. This creates microjets and enables droplets down to femtoliter volumes, resulting in spatial resolution in the sub- μm range, down to 100 nm.^[23] E-jet printing has been previously used to deposit silica nanoparticle suspensions with various structural colors being achieved through self-assembly pathways.^[24] E-jet has also been used to create microscale pixels of quantum dots, demonstrating its capabilities in creating optoelectronic devices.^[25] Recently, photopolymers have been deposited by e-jet for optical applications, albeit in simple, single layer configurations.^[26] In Part I of this companion paper set, the e-jet process parameters governing the creation of the multimaterial, multilayered structures is detailed.^[27] In Part II

of this companion paper set, the optical properties of the materials used in Part I are quantified and the photonic response of the printed 1DPCs are determined and tied back to capabilities of the processing method.

2. Results and Discussion

2.1. Material Selection Criteria for Additive Manufacturing of 1DPCs

2.1.1. Optical Criteria

Consider a generalized filter array illustrated in **Figure 1**. Varying the refractive index contrast between the materials in the stack controls the width of the stop band; low contrast allows for creation of narrow bands such as those used in notch filters, while higher contrast results in broadband reflectors. To

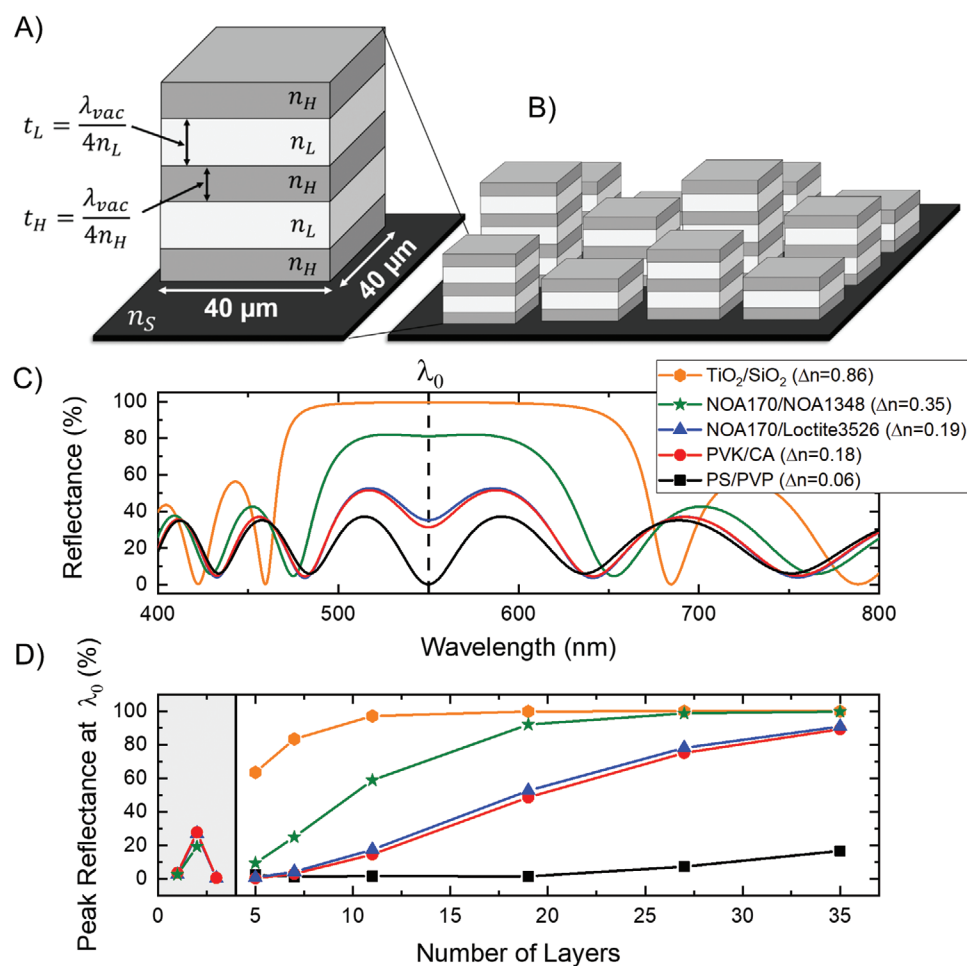


Figure 1. Optical design of printed 1DPCs. A) Diagram of a 1DPC with alternating layers of high (n_H) and low (n_L) refractive index polymers with the physical thickness of each layer (t_H , t_L) determined by the center wavelength (λ_0) as well as the refractive index of the layer. B) Proposed arbitrary array of various layer pair 1DPCs that would be created via the e-jet printing process. C) Reflection comparison of material combinations in Table S1 of the Supporting Information with the same number of alternating index layers ($N = 15$) centered at $\lambda_0 = 550$ nm demonstrating the increase in stop band width as well as reflectance with increasing refractive index contrast. The simulations are conducted using a high refractive index ($n_S = 3.98$) silicon substrate for more direct comparison to the printing process. D) Peak reflectance achieved at the center wavelength ($\lambda_0 = 550$ nm) for an ideal 1DPC for an increasing number of layers. The shaded region simulates one, two, and three-layer stacks which covers the extent of experimental data presented in this paper.

minimize parasitic absorption and a resulting loss in reflection, the materials selected should also have high transmission across the desired wavelength range.

Several trade-offs regarding ink composition need to be navigated in balancing process and application requirements. Titania (TiO_2) and silica (SiO_2) sol-gels have previously been used in dip-coated photonic crystals that achieved significant refractive index contrast of $\Delta n = 0.86$ ($n_{\text{TiO}_2} = 2.34$ and $n_{\text{SiO}_2} = 1.48$).^[28] Silica and titania-silica inks were also used in a direct-write AM process to produce optical quality glass components with varying refractive indices.^[29] In comparison, fluorinated polymers have refractive indices as low as $n \approx 1.3$, while those with large aromatic rings or sulfur groups can have indices as high as $n \approx 1.7$, yielding a contrast maximum of $\Delta n = 0.4$.^[30,31] In prior work, refractive index contrast in polymeric 1DPCs ranged from $\Delta n = 0.07$ for a polystyrene/polyvinylpyrrolidone (PS/PVP) combination to $\Delta n = 0.18$ for a polyvinyl carbazole/cellulose acetate (PVK/CA) combination.^[9,32] Photopolymers are a mature class of materials with a wide range of commercially available compositions, with refractive indices ranging from 1.315 (fluorinated acrylate polymers) to >1.70 (zirconia nanoparticle-doped acrylates).^[33,34] In terms of refractive index contrast, the polymeric systems discussed here are significantly lower than the sol-gel systems thus requiring more layers to achieve the same optical response. However, in the context of the e-jet printing apparatus, the ability to print multiple layers without having to remove the substrate is critical for both printing speed and reduction of errors due to reregistration when replacing the substrate. The oxide sol-gels require a multistep curing process, including annealing at over 400°C , while the PS/PVP and PVK/CA polymer combinations both require low temperature thermal cures around 100°C . By contrast, photopolymers typically require a sub-30 s exposure to UV light to solidify the film, thus allowing multiple layers to be cured in situ on the printing apparatus. The easier processability and relatively high refractive index contrast compared to benchmark

polymeric systems make photopolymers ideal candidates for use in a multilayer, multimaterial printed photonic crystal. Potential drawbacks to using polymers for optics, as opposed to more traditional ceramics, include higher susceptibility to heat and moisture and thus limit them from certain applications. The following photopolymers are investigated in this work: NOA170, a high index acrylate photopolymer doped with zirconia nanoparticles (average diameter 8–11 nm), Loctite 3526, a moderate index acrylate photopolymer, and NOA1348, a fluorinated low refractive index photopolymer. The cured refractive indices of these three materials are: 1.70, 1.51, and 1.35, respectively. Table S1 of the Supporting Information compares these photopolymers to the other candidate materials discussed above.

The reflection spectra of a hypothetical 15-layer photonic crystal are calculated for each material pair (Figure 1C) by solving the Fresnel equations using the transfer matrix method modified from previous work, illustrated here at a convenient center visible wavelength, $\lambda_0 = 550$ nm, of the 1DPC.^[35] Figure 1D demonstrates the increase in peak reflectance with an increasing number of alternating index layers, showing that a higher contrast allows the use of fewer layers to achieve a given level of reflectance. The proposed photopolymer combinations can achieve comparable or better reflectance response as those obtained in previously reported polymeric 1DPC systems.^[11] Specifically, the photopolymer combination of NOA170-Loctite has very similar optical characteristics to the polyvinyl carbazole-cellulose acetate (PVK-CA) combination. The spin-coated PVK-CA system was thus used as a model system for comparison to the printed structures described later in this paper.

Variable angle spectroscopic ellipsometry (VASE) and transmission spectroscopy were used to measure the refractive index and transmission across the visible to near infrared (NIR) (400–800 nm) spectrum ranges of the photopolymers (NOA170, NOA1348, Loctite 3526) and the thermally cured polymers (PVK and CA). These measurements are summarized in Figure 2. The manufacturer of the NOA materials provides refractive

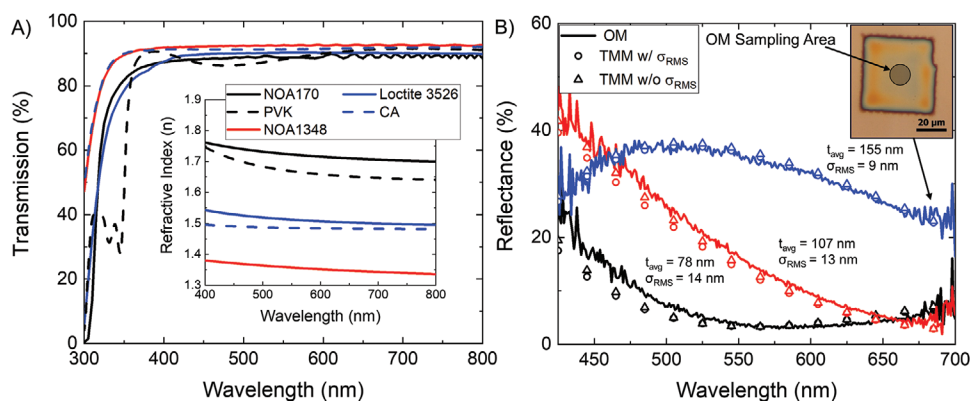


Figure 2. Optical properties of printed and spin-coated polymers. A) Optical transmission properties through NOA170, Loctite 3526, NOA1348, polyvinyl carbazole (PVK), and cellulose acetate (CA) with inset showing the refractive indices of the polymers. Samples were spin-coated onto glass substrates to a thickness of $2\ \mu\text{m}$ for all polymers. B) Reflectance spectra (colored traces) obtained from three samples of NOA170 on silicon collected using the optical microreflectance (OM) system. Transfer matrix method (TMM) optical simulations (triangles and circles) based on AFM-derived thicknesses show close matching across all samples. AFM-derived root mean square surface roughness (σ_{RMS}) surface roughness is included in the TMM simulations as well. Mean squared error (MSE) between the OM measurements and TMM including and excluding roughness are less than 10 showing the negligible effect of the low surface roughness on the measured response and simulations. (Inset) Optical image of a 155 nm thick printed NOA170 sample with $\approx 15\ \mu\text{m}$ sampling spot via the OM system indicated via the shaded circle. AFM data were taken for the entire sample but the roughness and thickness for simulations are taken from an overlapping area with the OM measurement. σ_{RMS} across the entire sample is ≈ 20 nm.

index values of 1.70 for NOA170, 1.51 for Loctite 3526, and 1.348 for NOA1348 at the sodium D line (589 nm). Measured values at 589 nm were: $n = 1.72$, 1.52, and 1.35 for NOA170, Loctite 3526, and NOA1348, respectively. The values of $n = 1.48$ and 1.66 for CA and PVK, respectively, also agree well with literature. Note that for films that are 100 nm thick, any large particle could lead to a significant amount of surface roughness. One of the inks studied, Loctite 3526, required filtering (using a 0.22 μm filter) to remove large oligomer entanglements or resin particles that can cause clogging of the small diameter nozzle prior to printing. A potential drawback to filtering the inks is that the refractive index or transmission properties may change as a result. For the Loctite, a slight drop in refractive index of 0.01 and an increase in transmission of 2% were observed, as summarized in Figure S1 of the Supporting Information. Overall, the measured refractive index contrast as well as high transmission across the visible to NIR spectrum (>80% for all materials tested) make these inks promising candidates for use in a printed photopolymer photonic crystal.

2.1.2. Interfacial Criteria

The goal of the printing process is to produce a thin, uniform layer of polymer over a defined area. Once a polymer is deposited and cured, it then becomes the substrate for the next layer. Whether a polymer will deposit effectively, and ultimately merge to form a film, is determined in part by the surface energy of both the liquid polymer and the solid surface. Generally, the first layer of a 1DPC is the higher refractive index material. Thus, the following cured-uncured polymer interactions must be understood: interaction between the high index photopolymer and the printing surface (here, silicon), interaction between the liquid lower index polymer on a cured higher index layer, and interaction between the liquid higher index polymer on a cured lower index layer. If these interactions are known, it is possible to predict which material combinations are likely to merge to a film using e-jet deposition. The results and discussion of solid surface energy and liquid surface tension at the macro- and microscale are detailed in Part I of this companion paper set. In summary, the relatively low solid surface energy of the low refractive index materials (here Loctite 3526 and NOA1348) coupled with the high liquid surface tension of the high refractive index material (NOA170) make it difficult to form a third layer (high index on low index). This is likely due to the low work of adhesion to the low surface energy polymer substrates as well as high work of cohesion of the NOA170 to itself, preventing the spreading of deposited ink. The low surface energy is likely due to the fluorinated groups used to decrease the effective refractive index of the low index photopolymer. The corresponding increase of film roughness due to partial merging, and its effect on the optical properties of the layers, is discussed further in the next section.

2.2. Printing and Characterization of Single and Multilayer Photopolymer Films

E-jet printing (see schematic in Figure 1 of Part I) is capable of printing high resolution patterns of multiple materials by

applying a high voltage (typically 200–1000 V) between a small diameter, conductive nozzle, and a grounded substrate. This forms what is known as a Taylor cone of material at the nozzle orifice which, when pulsed with a varying voltage, ejects a drop which is smaller than the diameter of the nozzle. There are several printing modes that are possible with the e-jet, including continuous cone-jet, multijet, and drop-on-demand. In drop-on-demand mode, the droplets are deposited at high frequency and then merge within milliseconds of contacting the surface to form first a line and then a film. Due to the extremely thin layers and high spatial resolution required for creating the 1DPCs in this work, drop-on-demand printing is selected for its droplet volume and placement precision. Other modes, such as the continuous cone-jet mode, would deposit excess material in one location and thus small, thin layers would be limited by stage speed. The spacing and sizing of the drops determines the resulting film thickness as well as surface roughness. In this work, a 1 μm nozzle is used with drop-on-demand printing. The droplets merge within milliseconds of contacting the surface to form first a line and then a film. Once an array of drops has been printed, the array is shuttled to a curing station where nitrogen gas is flowed over the surface and the surface is exposed to 365 nm UV light. The nitrogen gas is critical for full curing of NOA170 and 1348 as the photopolymerization reactions are oxygen-inhibited. For reference, the Loctite 3526 photopolymerization is not oxygen inhibited. The e-jet apparatus used to complete this work is outfitted with two nozzles, which provide several added benefits over a single nozzle system. Due to the bimaterial composition of the 1DPCs, a dual nozzle system allows for efficient switching between material sources, reducing registration errors caused by switching nozzles. The dual nozzle configuration also increases production throughput, which reduces evaporative clogging of the individual nozzles. Videos demonstrating deposition of a single layer onto a silicon substrate and deposition onto an already printed layer are provided in Movies S1 and S2 of the Supporting Information, respectively.

The printed single and multilayer films can be characterized by atomic force microscopy (AFM) and OM. The former is integrated directly into the printing apparatus and is used to determine film thickness as well as σ_{RMS} . The latter was configured as a modification of the design by Frisenda et al.,^[36] allowing the measurement of reflectance and transmission spectra with a spot size as small as 5 μm by coupling the focusing power of a microscope objective with the limiting aperture of a fiber optic cable. Here, a 10 \times or 50 \times objective coupled with a 50 μm multimode optical fiber is used. All reflectance spectra shown in the rest of this manuscript were taken using a 10 \times objective which results in a spot size of $\approx 15 \mu\text{m}$. A more detailed description of the system operation can be found in Figure S2 of the Supporting Information. To achieve an $\approx 100 \text{ nm}$ thick film, the droplet diameter deposited was typically between 1.0 and 2.5 μm , depending on the polymer being used. Thus, the 15 μm spot size covers ≈ 60 droplets and is an averaged measurement. The spatial resolution of the AFM is in the sub- μm range, however, and a comparison in surface roughness for an OM sampling area to the area of a single droplet can be used to better understand how the σ_{RMS} varies within the spot of the OM system. This is summarized in Figure S3 of the Supporting

Information. Generally, the variation in σ_{RMS} between sampling sizes was small (on the order of 5–10 nm) which have been shown to have little effect on optical response (see Figure 2B).

NOA170 was first deposited as a single uniform layer and process parameters were adjusted to modulate thickness and, therefore, optical response as shown in Figure 2B. Three printed samples were measured with both the AFM and OM, with the AFM-measured thicknesses of the three samples (78, 105, and 155 nm) obtained by modulating the spacing, or pitch, of the droplets, as detailed in Part I. These thicknesses, along with wavelength-dependent refractive index data, were then used as inputs for the TMM simulation. Reflectance spectra collected from 15 μm spots in the center of the AFM-scanned area matched closely to the simulation, suggesting that OM can be used to accurately determine film thickness in situ and more conveniently and rapidly than AFM.

A previous study used interfacial and surface roughness to model thickness as a Gaussian distribution to provide more accurate parameters for the transfer matrix solver and the simulation used in this work utilizes a similar method to account for surface roughness.^[37,38] The mean-squared error (MSE) is used to compare the TMM simulations to the measured spectra with a low MSE (for ellipsometry typically a value of <10) indicating a good fit. Both simulations (with and without roughness) were

compared to the measured spectra and differences between the two were found to be negligible with average MSE values of 6.3 and 4.2 including and excluding roughness, respectively.

The combinations (NOA170 + NOA1348) and (NOA170 + Loctite 3526) were tested as bilayers. Uniform layers of each are obtained at low thicknesses (<200 nm for both). Optical simulations, taking into consideration the index of each of the layers, were used to compare the measured reflectance spectra and close matching for both material sets are found. While both sets can be printed as bilayers, Loctite 3526 formed more uniform films than NOA1348, and thus is used to demonstrate the ability to create an all-printed Bayer filter array, as summarized in Figure 3. For reference, the results from the NOA170 + NOA1348 study are summarized in Figure S4 of the Supporting Information.

The standard Bayer array is composed of pixelated color filters of which 50% are for filtering green light and 25% are for red and blue light, respectively. To match the color response of these filters, it is possible to design for peak reflectance at certain parts of the spectrum by varying the thickness of the high and low index materials independently. The thicknesses of each layer gathered via AFM are summarized in Table 1 as well as average RMS roughness values. The close matching between the TMM simulation using the AFM-measured thicknesses

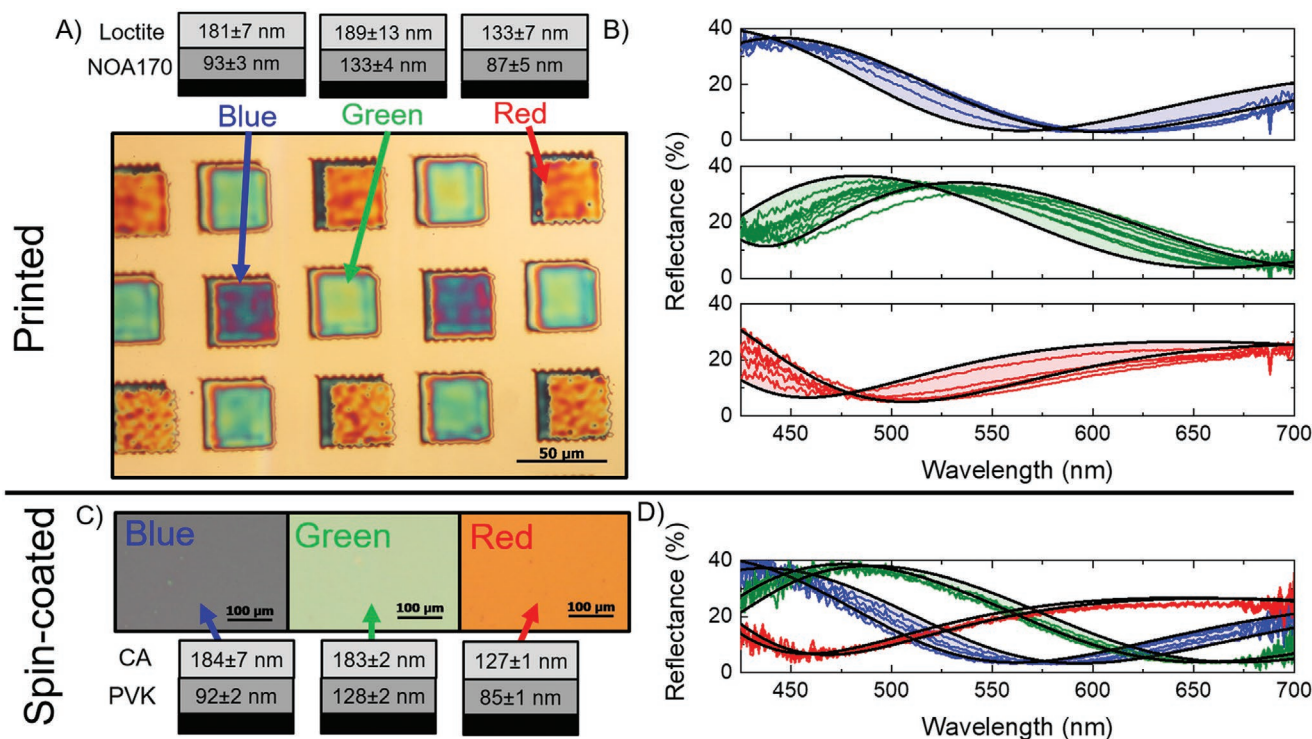


Figure 3. Printed Bayer filter bilayers optical image (50 \times) of printed Bayer array composed of NOA170-Loctite 3526 dual layers demonstrating uniformity of pixel size (40 μm \times 40 μm) and color with blue, green, and red reflected light visible. Thicknesses of each layer along with standard deviations across all samples ($N = 4$ to 9) for each color pixel are denoted in the graphic above and in Table 1. B) OM results of all of Row 2 and Row 3 (9 samples each) matching visual determination of reflected colors in (A). Simulations (shaded region) based on high and low error (plus/minus thickness variation in (A) in all three dual layers shows good bounding of all measured samples. The TMM simulations incorporate σ_{RMS} roughness as determined by AFM. C) Optical response comparison of printed NOA170-Loctite stacks with spin-coated PVK-CA dual layers ($N = 5$). Due to the almost identical refractive index contrast, spin-coated stacks with similar thicknesses show similar optical response. Process variation (plus/minus thicknesses) and surface roughness (between 2 and 10 nm) for the spin-coated layers was lower and there was a resulting closer bound to the measured data (TMM given as black lines in (D)).

Table 1. Geometric and optical comparison between e-jet printed (NOA170-Loctite 3526) and spin-coated (PVK-CA) samples in Figure 3.

E-jet printed Layer 1: NOA170 Layer 2: Loctite	Layer 1 thickness [nm]	Layer 1 σ_{RMS} [nm]	Layer 2 thickness [nm]	Layer 2 σ_{RMS} [nm]	Peak reflectance [%]	Peak reflectance [nm]
Blue ($N = 4$)	92.7 ± 3.1	8.0 ± 0.4	180.9 ± 6.5	12.8 ± 1.5	37.9 ± 0.9	430.5 ± 4.0
Green ($N = 9$)	132.8 ± 3.6	8.8 ± 1.3	189.2 ± 12.5	17.8 ± 3.4	33.4 ± 1.2	514.1 ± 15.0
Red ($N = 5$)	86.7 ± 5.1	9.3 ± 1.1	132.5 ± 7.3	17.7 ± 4.6	25.1 ± 1.0	688.8 ± 6.5
Spin-coated Layer 1: PVK Layer 2: CA						
Blue ($N = 5$)	92.0 ± 1.5	5.5 ± 1.4	183.9 ± 6.9	-0.6 ± 1.4	42.5 ± 0.7	436.2 ± 7.2
Green ($N = 5$)	128.2 ± 2.4	-0.6 ± 2.6	183.1 ± 1.7	0.8 ± 1.6	40.2 ± 0.7	468.0 ± 11.2
Red ($N = 5$)	84.7 ± 1.1	9.7 ± 0.9	127.1 ± 1.4	0.1 ± 1.8	25.7 ± 0.1	675.6 ± 3.4

and the optical reflectance is consistent over a relatively large sample size ($N = 18$), demonstrating the repeatability of the manufacturing technique. Uniform spectral response across a single pixel is also critical. This was investigated thoroughly in Figure 4. The OM system was utilized to take five samples, one in the center and four corners, of blue, green, and red pixels as indicated in the optical images. Generally, the peak reflectance of the blue and red samples had low standard deviations in location not exceeding a 10 nm shift. There was a larger shift in the green samples, up to 18 nm, which is attributable to the higher degree of variation in thickness across these samples. Peak reflectance values for these samples can be found in Table S2 of the Supporting Information. To benchmark the printed samples, dual layers of spin-coated PVK-CA were designed and fabricated to have a similar optical response to the printed structures. These results are shown in Figure 3C,D. Under the same illumination conditions, there is a qualitative match between the microscale printed samples and macroscale spin-coated samples. In addition, Table 1 provides a quantitative comparison in peak reflectance between the e-jet printed

and spin-coated samples. Overall, there was an 11% decrease in peak reflectance in e-jet printed samples; attributed to the higher degree of surface roughness and resultant scattering loss. There was, however, a comparable standard deviation in peak reflectance position across all samples, driven by relatively low variation in thickness of 6.5 and 2.5 nm for printed and spin-coated samples, respectively.

It is noted that the relatively poor thickness control over the blue PVK/CA spin-coated sample compared to the green and red samples was likely due to the model developed to deposit the dual layers being less accurate at the higher CA solution concentrations and slower spin speeds. Furthermore, only a limited number of samples were created for analysis; with a larger number of samples, the deviation is expected to decrease. The empirical model used to deposit the PVK/CA dual layers is shown in Figure S5 of the Supporting Information.

When manufacturing optical structures such as 1DPCs, precise requirements must be met to achieve the desired photonic response. For example, the thickness of both the high and

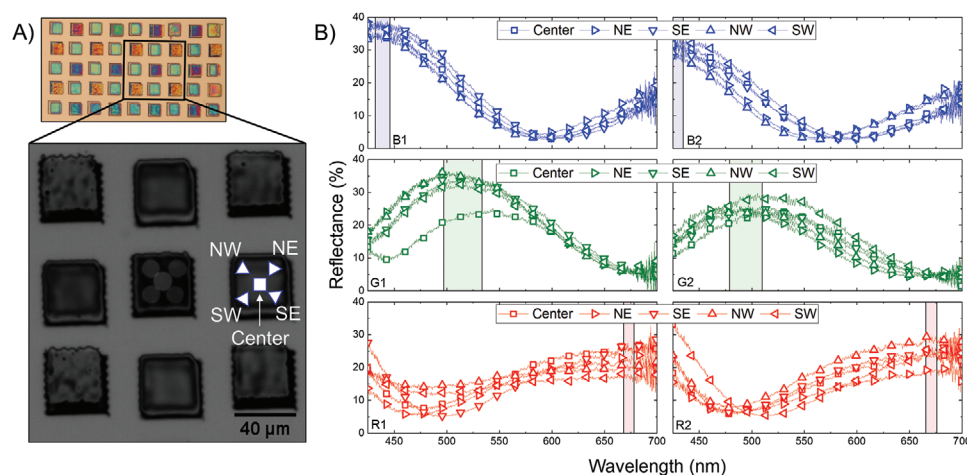


Figure 4. Spatial variation in pixel reflectance. A) Optical image of Bayer filter array with zoomed region indicating the locations across the area of a specific pixel that were measured using the OM system. Circles overlaid on the central sample show exact locations of data collection while the square/triangle symbols indicate the locations (center, NW, SW, NE, SE) of corresponding information in the reflectance plots. B) Reflectance spectra of two samples each of blue, green, and red samples. Shaded regions indicate the standard deviation in peak reflectance location for each sample. The larger reflectance variation in the green samples can be attributed to larger thickness variations in layer 2 (Loctite 3526) as compared to the red and blue samples.

low index layers must be maintained in a repeating fashion throughout the entire multilayered structure to generate constructive interference. In previous work, stochastic modeling of 1DPCs showed that the uncertainty in thickness of both the high and low index layers needs to remain within 10% of the design thickness (above or below) to maintain crystal functionality.^[39] In Table 1, the maximum plus and minus thickness deviation for any printed layer was for the second layer in the green samples at 12.5 nm. For a 189 nm thick film, that is a 7% deviation in thickness, thus falling within the 10% functionality threshold. The σ_{RMS} at the interfaces of a 1DPC has also been investigated for its effect on reflectance response and, for 1DPCs covering the visible and NIR, the reflectance remained constant for σ_{RMS} values under 20 nm.^[40] Thus, for this work covering visible and NIR 1DPCs, a threshold of 20 nm is set as an acceptable limit. Returning to Table 1, the maximum measured σ_{RMS} was 177 ± 4.6 nm which, taking into consideration the standard deviation, is near the roughness limit set. This is also comparable to the PVK-CA system which exhibited a maximum σ_{RMS} of 9.7 ± 0.9 nm. It should be noted that the printed samples were created without integrated process control and thus thickness variation as well as surface roughness are expected to decrease with further control development.

This work also sets forth a framework by which pixelated arrays of 1DPCs can be created. In high resolution imaging, for example, the size and sharpness of optical filtering elements is critical to achieving overall system capabilities. An ideal manufacturing process would be able to deposit layers composed of perfect rectangular prisms stacked on top of each other. Consider the “blue” patterns in Figures 3 and 4. The designed height for layers 1 and 2 were 90 and 180 nm, respectively. The designed in-plane dimensions were $40 \mu\text{m}$ by $40 \mu\text{m}$. The cross-sectional profile of the deposits was measured by AFM and compared to the “ideal” structure in Figure S6 of the Supporting Information.

A parameter such as the deposit shape factor, η , can be used to quantify the deviation between ideal and manufactured deposits, with a value of zero being a perfect deposit.^[41] We find that $\eta = 0.14$ for the second layer, greater than the $\eta = 0.06$ found for the first layer, attributed to the challenge in depositing onto a relatively rough printed polymer surface. Furthermore, the tapering in the first layer led to a smaller printing area available for the second layer. Thus, spatial analysis of the printed pixels was also conducted to quantifying the capabilities of the manufacturing technique. Deviations from designed ideal spatial values for the $40 \times 40 \mu\text{m}^2$ square pixels were 0.8%, whereas $13 \times 13 \mu\text{m}^2$ pixels exhibited deviations of 4.4%. The larger spreading of smaller pixels is attributed to challenges in balancing thickness and spatial requirements. This analysis is shown in Figure S7 of the Supporting Information. In both cases, the results suggest that the e-jet printing can achieve industrially relevant, patterned 1DPCs with acceptable error in thickness, surface roughness, pixel sharpness, and spatial area coverage.

Based on the surface studies summarized earlier, the challenge in creating a layered structure for this system is overcoming the lower solid surface energy of NOA1348 and Loctite as well as the high liquid surface tension of NOA170. In practice, it was found that the NOA170 ink would not merge into a film on top of NOA1348 but would partially merge into

a thin film on Loctite. (The poor merging behavior of NOA170 on NOA1348 is depicted in Figure S4A, Supporting Information.) We hypothesize that the higher liquid surface tension NOA170 ink is more likely to cohere to itself versus adhere to a low solid surface energy surface like Loctite or NOA1348. The slightly higher solid surface energy of the filtered Loctite over NOA1348, 19.4 and 11.5 mN m^{-1} , respectively, might also explain the preferential merging characteristics. **Figure 5** demonstrates a semiuniform layer of NOA170 deposited on top of Loctite, as demonstrated by the relatively high roughness of the third layer ($\sigma_{\text{RMS}} > 30$ nm). As evidenced by the measured spectra, the roughness can result in a significant reduction in the reflectance response due to light scattering. This is further confirmed by comparing the printed sample to the response of a spin-coated sample of equal layer thickness. The surface roughness was below 10 nm for all three layers in the PVK-CA sample and thus there was low scattering loss. As these results indicate, it is possible to derive both thickness and roughness data from OM scans more rapidly than from AFM scans. While surface roughness is the likely cause of reflection loss in these samples, there are other potential sources of optical loss. Due to the multilayered and multimaterial nature of the 1DPCs, there is also a potential for contraction of the photopolymers, particularly during the curing process. For example, previous reports have demonstrated that multilayered, UV-cured acrylics show significant warping at the millimeter scale.^[42] Any variation in thickness due to warping could significantly affect the optical performance of the 1DPCs. However, there was no noticeable warping detected in the microscale printed multilayers, which may be attributed length scale dependence of the behavior. Once cured, the photopolymers investigated here are quite durable. Developed as adhesives, the shore durometer of the NOA170 and Loctite 3526 are 75 and 62, respectively. For a frame of reference, the shore durometer of a high-density polyethylene hard hat is ≈ 75 . To show the durability of the optical performance of these printed photopolymer 1DPCs, reflectance measurements are taken from several samples over one year after they were manufactured and only minor shifts in the spectra were observed. This comparison can be found in Figure S8 of the Supporting Information.

Overall, the thicknesses of the layers being deposited (between 80 and 200 nm) are in the optimal range for NIR 1DPCs near the boundary of the visible regime. A 7-layer 1DPC with similar thicknesses as in Figure 4 ($t_{\text{H}} = 100$ nm and $t_{\text{L}} = 145$ nm) would have a peak reflectance of around 35% at 780 nm (if the sample were deposited on glass). Based on the transmission results gathered, these materials will still have good transparency at these longer wavelengths and thus these photonic crystals could find applicability in an array of NIR optical devices.

3. Conclusions

In this work, photopolymeric materials with refractive indices near the boundaries of understood organic maximums were investigated for use as the constituent materials in 1D photonic crystals. Criteria for selecting appropriate material pairs, based on a negotiation of optical and interfacial characteristics, were

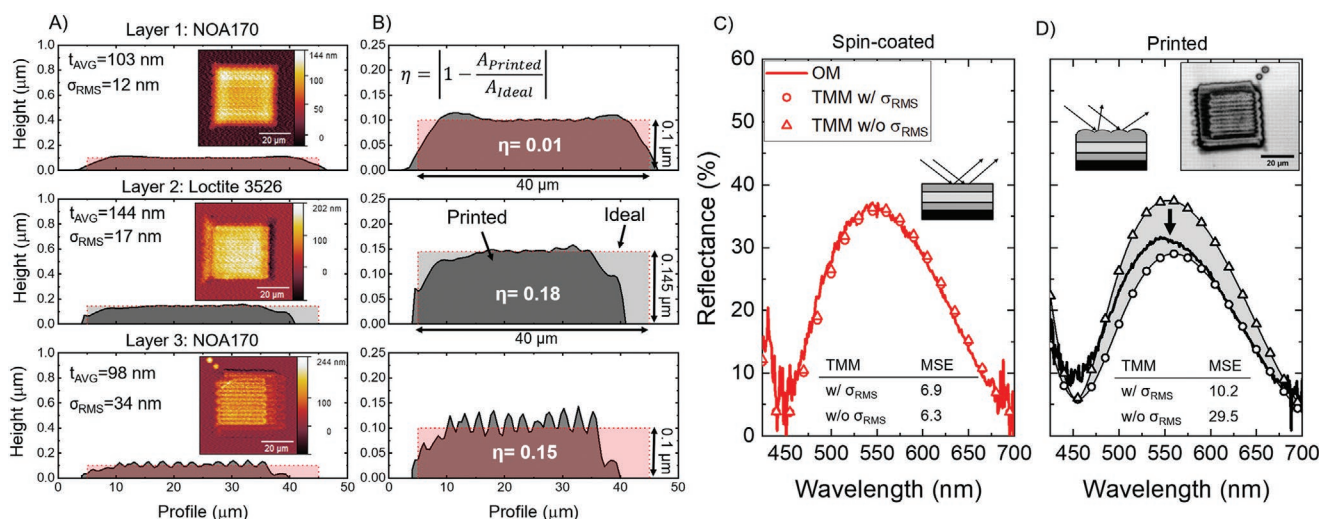


Figure 5. Trilayer 1DPC. A) AFM-generated cross-sections of printed NOA170/Loctite 3526/NOA170 trilayer pixel with average layer thickness, surface roughness, and top view AFM in inset. B) Zoomed cross-sections of printed layers showing ideal thickness (100 nm/145 nm/100 nm) and base profile for each layer along with the deposit shape factor, η . A high degree of surface roughness can be seen in the third NOA170 layer. C) Reflectance spectra and TMM of three layered sample of PVK/CA/PVK (102 nm/146 nm/100 nm) showing low MSE between the TMM and OM spectra due to low surface roughness ($\sigma_{RMS} < 10$ nm) in all three layers. D) Reflectance spectra and TMM of NOA170/Loctite 3526/NOA170 with image in inset. Inclusion of roughness in TMM simulations results in a closer match to the optical spectra with MSE between the optical response and simulation with roughness being 10.2 versus 29.5 for the simulation without roughness. The drop in reflectance is attributed to scattering resulting from a high degree of surface roughness in the third printed layer.

identified as well. Photopolymers with high refractive index contrast and good transmission were selected for ease of processing on the printing platform. In Part I of this companion paper set, interfacial materials selection criteria were presented showing that drops of photopolymer ink are more likely to merge to uniform layers on high solid surface energy substrates (i.e., NOA170 and silicon), while the high liquid surface tension of NOA170 prevents good adhesion to low solid surface energy substrates such as NOA1348 and Loctite. Electrohydrodynamic jet printing was investigated as a platform for depositing these photopolymers in precise 3D space with μm resolution in X and Y and nanometer resolution in Z . Printed structures were shown with layer thicknesses from 80 to 200 nm, which allowed for modulation of light directly in the NIR (700–1000 nm) and a significant portion of the visible spectrum (400–700 nm). Surface roughness, due to incomplete merging of a single layer, was high compared to other polymeric 1DPCs reported previously, yet still suitable for realizing dielectric mirrors and filters. Future studies will focus on decreasing surface roughness through investigating the trade-off between refractive index contrast and favorable surface energetics. Continued development could facilitate coupling polymeric 1DPCs with optoelectronic devices. For example, it is now foreseeable that a customized, all-printed array of 1DPCs for wavelength selection could be realized directly on a CMOS circuit, eschewing masks or solvents, thus addressing an issue with spatial and spectral resolution trade-off in the hyperspectral imaging community.^[43] Furthermore, and more in line with previous polymer-based 1DPC developments, this method could allow for a large number of customized optical sensors to be printed onto a single chip; finding applications in fields ranging from bio-analyte to gas sensing.^[44]

4. Experimental Section

Photopolymer Properties and Curing: Photopolymers are sourced from Norland Products (Cranbury, NJ) and Henkel Corporation (Düsseldorf, Germany). Norland Optical Adhesive 170 (NOA170) has a viscosity around 5000 cP at 25 °C while NOA1348 has a viscosity around 1600 cP at 25 °C. Loctite 3526 has a manufacturer supplied viscosity of 17 500 cP at 25 °C. Rheological properties were measured using a TA Instruments DHR-3 rheometer. Printed samples were cured on the e-jet printing setup using a 365 nm UV LED lamp as well as a nitrogen flow over the surface to prevent oxygen inhibition of the photopolymerization process. All photopolymers were filtered using a 0.2 μm filter prior to printing.

Optical Simulations and Measurements: Refractive index values for all polymers studied were obtained from spin-coated films using a J.A. Woollam M-2000 VASE using wavelengths from 400 to 1200 nm and angles from 55° to 75°. Samples for transmittance measurements were spun-coat onto glass microscope slides at varying speeds depending on the polymer viscosity and then taken from 300 to 900 nm using a Perkin-Elmer Lambda 650 Spectrophotometer. Sample thickness was kept consistent at 2 μm . Microreflectance measurements were obtained using the custom setup further detailed in the supplementary material. All these measurements were taken using a ≈ 10 μm spot size using the 10 \times objective. Transfer matrix simulations were carried out using the RefDex open source software (University of Duisburg-Essen). Wavelength-dependent optical constants collected for the silicon wafer, NOA170, NOA1348, Loctite 3526, PVK, and CA were used as inputs for RefDex along with AFM-derived surface roughness. The surface roughness of spin-coated PVK and CA films were taken as an average of five spots via the VASE.

Topography Characterization: Atomic force microscopy measurements were taken using a Nanosurf NaniteAFM integrated directly onto the printing setup and the data was postprocessed using Gwyddion software using a 1D FFT filter (to account for noise generated in the translational stage).

Supporting Information

Supporting Information is available from the Wiley Online Library or from the author.

Acknowledgements

The authors would like to acknowledge Steve Morris, Erin Evke, and Chris Pannier for helpful conversations and the Tuteja Research Lab at the University of Michigan for support and guidance on completing the interfacial studies. This work was supported by the National Science Foundation (CMMI 1727894).

Conflict of Interest

The authors declare no conflict of interest.

Keywords

additive manufacturing, multimaterials, photonic crystals, photopolymers

Received: May 5, 2020

Revised: July 14, 2020

Published online: August 26, 2020

- [1] J. L. Jewell, A. Scherer, S. L. McCall, Y. H. Lee, S. Walker, J. P. Harbison, L. T. Florez, *Electron. Lett.* **1989**, 25, 1123.
- [2] P. H. Lissberger, W. L. Wilcock, *J. Opt. Soc. Am.* **1959**, 49, 126.
- [3] I. R. Howell, C. Li, N. S. Colella, K. Ito, J. J. Watkins, *Appl. Mater. Interfaces* **2015**, 7, 3641.
- [4] P. Lova, G. Manfredi, L. Boarino, A. Comite, M. Laus, M. Patrini, F. Marabelli, C. Soci, D. Comoretto, *ACS Photonics* **2015**, 2, 537.
- [5] K. Lee, S. A. Asher, R. V. June, *J. Am. Chem. Soc.* **2000**, 122, 9534.
- [6] P. Bhattacharya, H. Gebretsadik, O. Qasaimeh, K. K. Kamath, C. Caneau, R. J. Bhat, *Proc. SPIE* **1999**, 3627, 112.
- [7] N. Anderson, P. Prabhat, T. Erdogan, *Proc. SPIE* **2012**, 8226, 1.
- [8] D. Comoretto, *Organic and Hybrid Photonic Crystals*, Springer, New York, NY **2015**.
- [9] G. Manfredi, P. Lova, F. Di Stasio, R. Krahn, D. Comoretto, *ACS Photonics* **2017**, 4, 1761.
- [10] K. D. Singer, T. Kazmierczak, J. Lott, H. Song, Y. Wu, J. Andrews, E. Baer, A. Hiltner, C. Weder, *Opt. Express* **2008**, 16, 10358.
- [11] P. Lova, G. Manfredi, D. Comoretto, *Adv. Opt. Mater.* **2018**, 6, 1800730.
- [12] H. Shen, Z. Wang, B. Yang, *RCS Adv* **2016**, 6, 4505.
- [13] Y. Horie, A. Arbabi, E. Arbabi, S. M. Kamali, A. Faraon, *Opt. Express* **2016**, 24, 11677.
- [14] M. Lequime, L. Abel-Tiberini, K. Mathieu, J. Berthon, J. Lumeau, *Proc. SPIE* **2015**, 9627, 1.
- [15] J. Lumeau, F. Lemarquis, T. Begou, K. Mathieu, I. Savid De Larclause, J. Berthon, in *ICSO 2016 Int. Conf. on Space Optics Filters* (Eds: B. Cugny, N. Karafolas, Z. Sodnik), ICSO, Biarritz, France **2016**.
- [16] A. Boltasseva, V. M. Shalae, *Metamaterials* **2008**, 2, 1.
- [17] A. Camposeo, L. Persano, M. Farsari, D. Pisignano, *Adv. Opt. Mater.* **2019**, 7, 1800419.
- [18] B. M. Boyle, T. A. French, R. M. Pearson, B. G. McCarthy, G. M. Miyake, *ACS Nano* **2017**, 11, 3052.
- [19] J. J. Schwartz, A. J. Boydston, *Nat. Commun.* **2019**, 10, 791.
- [20] K. Kowsari, S. Akbari, D. Wang, N. X. Fang, Q. Ge, *3D Print. Addit. Manuf.* **2018**, 5, 185.
- [21] Y. Liu, H. Wang, J. Ho, R. Ng, R. Ng, V. Hall-Chen, E. Koay, Z. Dong, H. Liu, C. Qiu, J. Greer, J. Yang, *Nat. Commun.* **2019**, 10, 4340.
- [22] J. Wang, L. Wang, Y. Song, L. Jiang, *J. Mater. Chem. C* **2013**, 1, 6048.
- [23] S. Mishra, K. L. Barton, A. G. Alleyne, P. M. Ferreira, J. A. Rogers, *J. Micromech. Microeng.* **2010**, 20, 095026.
- [24] H. Ding, C. Zhu, L. Tian, C. Liu, G. Fu, L. Shang, Z. Gu, *ACS Appl. Mater. Interfaces* **2017**, 9, 11933.
- [25] G. G. See, L. Xu, E. Sutanto, A. G. Alleyne, R. G. Nuzzo, B. T. Cunningham, *Appl. Phys. Lett.* **2015**, 107, 051101.
- [26] E. Sutanto, Y. Tan, M. S. Onses, B. T. Cunningham, A. Alleyne, *Manuf. Lett.* **2014**, 2, 4.
- [27] Z. Afkhami, B. Iezzi, D. Hoelzle, M. Shtein, K. Barton, *Adv. Mater. Technol.* **2020**, 5, 2000386.
- [28] M. Barhoum, J. M. Morrill, D. Riassetto, M. H. Bartl, *Chem. Mater.* **2011**, 23, 5177.
- [29] J. F. Destino, N. Dudukovic, M. Johnson, D. Nguyen, T. Yee, G. Egan, A. Sawvel, W. Steele, T. Baumann, E. Duoss, T. Suratwala, R. Dylla-Spears, *Adv. Mater. Technol.* **2018**, 3, 1700323.
- [30] W. Groh, A. Zimmerman, *Macromolecules* **1991**, 24, 6660.
- [31] T. Higashihara, M. Ueda, *Macromolecules* **2015**, 48, 1915.
- [32] J. Bailey, J. S. Sharp, *Eur. Phys. J. E* **2010**, 33, 41.
- [33] T. Norland/Norland Optical Adhesives **2019**.
- [34] S. Kudo, K. Nagase, S. Kubo, O. Sugihara, M. Nakagawa, *Jpn. J. Appl. Phys.* **2011**, 50, 06GK12.
- [35] T. D. Milster, *Topical Meeting on Optical Data Storage – Digest of Technical Papers*, College of Optical Sciences, University of Arizona, Tucson, AZ **1997**, p. 60.
- [36] R. Frisenda, Y. Niu, P. Gant, A. Molina-Mendoza, R. Schmidt, R. Bratschitsch, J. Liu, L. Fu, D. Dumcenco, A. Kis, D. Perez De Lara, A. Castellanos-Gomez, *J. Phys. D: Appl. Phys.* **2017**, 50, 074002.
- [37] K. Unger, R. Resel, C. Czibula, C. Ganser, C. Teichert, G. Jakopic, G. Canazza, S. Gazzo, D. Comoretto, *ICTON: 16th Int. Conf. on Transparent Optical Networks*, ICTON, Graz, Austria **2014**, pp. 1–4.
- [38] G. Yin, C. Merschjann, M. Schmid, *J. Appl. Phys.* **2013**, 113, 21.
- [39] M. I. Wafa, Y. M. El-Batawy, S. A. El-Naggar, *Optik* **2020**, 208, 164106.
- [40] I. A. Lujan-Cabrera, C. F. Ramirez-Gutierrez, J. D. Castaño-Yepes, M. E. Rodriguez-Garcia, *Phys. B* **2019**, 560, 133.
- [41] M. Shtein, P. Peumans, J. B. Benziger, S. R. Forrest, *J. Appl. Phys.* **2003**, 93, 4005.
- [42] D. Karalekas, A. Aggelopoulos, *J. Mater. Process. Technol.* **2003**, 136, 146.
- [43] L. Frey, L. Masarotto, M. Armand, M.-L. Charles, O. Lartigue, *Opt. Express* **2015**, 23, 11799.
- [44] K. Reddy, Y. Guo, J. Liu, W. Lee, M. Oo, X. Fan, *Lab Chip* **2012**, 12, 901.